

Noninvasive Method To Obtain Input Function for Measuring Tissue Glucose Utilization of Thoracic and Abdominal Organs

Tohru Ohtake, Noboru Kosaka, Toshiaki Watanabe, Ikuo Yokoyama, Toshiyuki Moritan, Masatoshi Masuo, Masahiko Iizuka, Kenji Kozeni, Toshimitsu Momose, Shinya Oku, Junichi Nishikawa, Yasuhito Sasaki, and Masahiro Iio

Department of Radiology, The Second Department of Internal Medicine, Department of Thoracic surgery, University of Tokyo, Tokyo, Japan

We have developed a method for the noninvasive estimation of regional tissue glucose utilization in humans that employs positron emission tomography (PET) and 2-(¹⁸F)fluoro-2-deoxy-D-glucose (FDG). Unlike other methods, the input function used in this method is obtained from the corrected time-activity curve of the descending aorta, not the left ventricle, because the descending aorta is relatively free of spillover from other organs and extends from the upper thorax to the lower abdomen. With this method the time-activity curve of the descending aorta must be corrected for the partial volume effect and the difference in counts between plasma and whole blood. Using the noninvasively obtained input function, regional tissue glucose utilization was calculated by Patlak graphic analysis. $k_1k_3/(k_2 + k_3)$ was in good agreement with $k_1k_3/(k_2 + k_3)$ calculated from the plasma input function by arterial sampling ($r = 0.9995$). These results suggest that the input function and regional tissue glucose utilization (not only of myocardium but also of other thoracic and abdominal organs) can be determined noninvasively.

J Nucl Med 1991; 32:1432-1438

2-(¹⁸F)fluoro-2-deoxy-D-glucose (FDG) was first used in positron emission tomography (PET) imaging of the myocardium by Phelps et al. (1). Many early myocardial PET studies were based on the qualitative evaluation of regional FDG uptake and its relation to flow (2-5). However, quantification of regional glucose utilization in the myocardium seemed to hold the potential for providing more reliable information about myocardial viability and cardiomyopathy.

A three-compartment FDG kinetic model for cerebral tissues was introduced by Sokoloff et al. (6). This model was used with PET to estimate local cerebral glucose

metabolic rates in humans. Patlak graphic analysis (7-8) and standard nonlinear regression (curve fitting) methods were used to quantify cerebral glucose metabolic rates (9). The latter two methods could be applied to heart, lung, kidney, and other thoracic and abdominal organs.

Sokoloff's autoradiographic method, however required static PET data and arterial blood sampling and the latter two methods required dynamic PET data and arterial blood sampling. Frequent arterial blood sampling is troublesome for both patients and investigators. A method using arterialized venous blood was developed by Huang et al. (10), but frequent sampling was again a problem for the investigators.

The purpose of our study is to present a noninvasive method for quantifying local glucose metabolic rates in thoracic and abdominal organs. A simple noninvasive method has already been developed by Gambhir et al (UCLA group), in which a time-activity curve of left ventricle blood pool is used as the input function (11). Gambhir's method, however, could only be applied to the heart, correction for spillover from myocardium to LV blood pool was difficult, and the correction for the difference between plasma and whole blood was, in our opinion, inadequate. Thus, we made an attempt to improve these points by using the corrected time-activity curve of the descending aorta as the input function.

MATERIALS AND METHODS

Preparation of FDG

FDG was synthesized by the method described previously by Ehrenkaufer et al. (12). The radiochemical purity was over 95%.

Human Subjects and Blood Sampling

Four patients with dilated cardiomyopathy (DCM), four with ischemic heart disease (IHD), one with hypertensive diffuse hypertrophy with IHD and one with mitral stenosis (46-76 yr of age) were studied. Each patient was informed as to the investigative nature of the study and its potential risks and benefits before informed consent was obtained. The study protocol had

Received May 23, 1990; revision accepted Dec. 17, 1990.

For reprints contact: Tohru Ohtake, Department of Radiology, University of Tokyo, 7-3-1 Hongo Bunkyo-ku, Tokyo, Japan.

been approved by the University of Tokyo's Human Subject Protection Committee.

Each patient had a carbohydrate meal 4–5 hr before the study. FDG (2–8 mCi) was then injected intravenously over a 30–60-sec period. Arterial samples (3 ml) from an arterial line and blood samples from a venous line were withdrawn at specific intervals. To define the time course of equilibration of ^{18}F activity between red blood cells and plasma, all blood samples were divided into two aliquots. Fluorine-18 activity in whole blood and in plasma was measured in a well counter and corrected for radioactive decay. Plasma glucose concentrations were measured at the beginning, middle and end of the study using standard enzymatic techniques.

Image Acquisition

The patients were studied using a Headtome IV PET scanner (Shimadzu Corp., Kyoto, Japan) with seven imaging planes, in which in-plane resolution was 4.5 mm at FWHM, axial resolution was 9.5 mm at FWHM and sensitivity was 14 and 24 kcps ($\mu\text{Ci}/\text{ml}$), respectively, for direct and cross planes (13). In all studies, transmission images were acquired in order to correct photon attenuation prior to obtaining the PET emission images. Nineteen dynamic scans were obtained during a 60-min 45-sec period using the following protocol: five 15-sec, three 30-sec, four 120-sec, four 300-sec and three 600-sec scans (Fig. 1).

Calibration and Image Processing

To obtain a calibration factor relating tomographic measurement of myocardial activity to blood sample activity obtained from the well counter, a cylindrical phantom (20 cm diameter) containing ^{68}Ga was scanned within a few days of the study. A

known volume of activity from the cylinder was also counted in the well counter. This provided the calibration between cts/min/pixel obtained from the PET images and cts/min/ml obtained from the well counter. All values obtained from PET were converted to cts/min/ml.

Cross-sectional images were reconstructed and corrected for the physical decay of ^{18}F to the FDG injection time. Myocardial tissue time-activity curves were obtained as follows. Five rectangular ROIs 6 mm² were defined on myocardium of the middle plane, as shown in Figure 2. Regions of interest (ROIs) were set on the final image of the dynamic scan and then applied to all previous images.

To calculate input function noninvasively, a rectangular ROI 6 mm² was set in the descending aorta on the fourth or fifth image of the dynamic scan on all seven planes to obtain aortic time-activity curves, each of which had nineteen point values (Fig. 3). All seven curves were smoothed after peaking by three-point smoothing to eliminate statistical noise.

As shown in Figure 3, the later phase of the left ventricular time-activity curve is shifted upward by spillover from the myocardium, whereas the aortic curves are almost entirely free of this effect. When the aortic diameter was not large enough, the count of these aortic curves was decreased by the partial volume effect. In addition, the curves do not represent plasma count but whole blood count. Thus, the aortic curves have to be corrected for both partial volume effect and the difference between whole blood and plasma counts.

We defined six sets of constants to correct venous whole blood count-to-arterial count (M_{ij} , Table 1 in Appendix A). The definition of M_{ij} is shown in the following equation:

$$M_{ij} = A_i/V_i, \quad \text{Eq. 1}$$

where A_i is arterial whole blood count at time i , V_i is venous whole blood count at time i , and M_{ij} is the ratio between arterial and venous whole blood counts at time i in j set.

We defined the ratio of arterial whole blood count to the

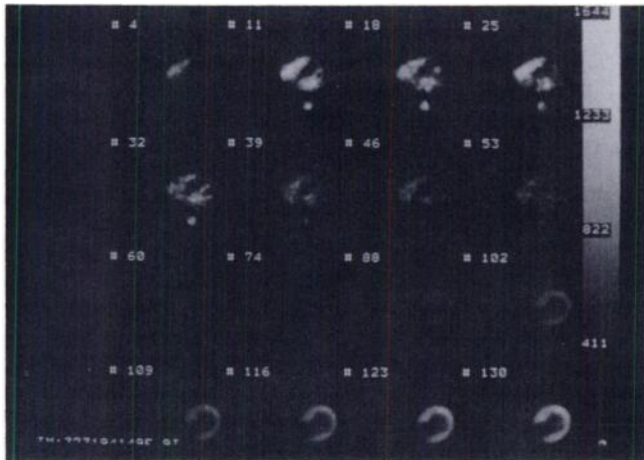


FIGURE 1. FDG radioactivity images obtained from a dynamic study of a patient with hypertensive diffuse hypertrophy. Frame 4: 0–15 sec; 11: 15–30 sec; 18: 30–45 sec; 25: 45–60 sec; 32: 1 min–1 min 15 sec; 39: 1 min 15 sec–1 min 45 sec; 46: 1 min 45 sec–2 min 15 sec; 53: 2 min 15 sec–2 min 45 sec; 60: 2 min 45 sec–4 min 45 sec; 74: 4 min 45 sec–6 min 45 sec; 88: 8 min 45 sec–10 min 45 sec; 102: 10 min 45 sec–15 min 45 sec; 109: 20 min 45 sec–25 min 45 sec; 116: 30 min 45 sec–40 min 45 sec; 123: 40 min 45 sec–50 min 45 sec; 130: 50 min 45 sec–60 min 45 sec. The activity is first primarily that of right heart, it then shifts to the left ventricle and descending aorta. As blood-pool activity decreases, that of myocardium increases. The time-activity curves for the descending aorta and myocardium were obtained from these images.

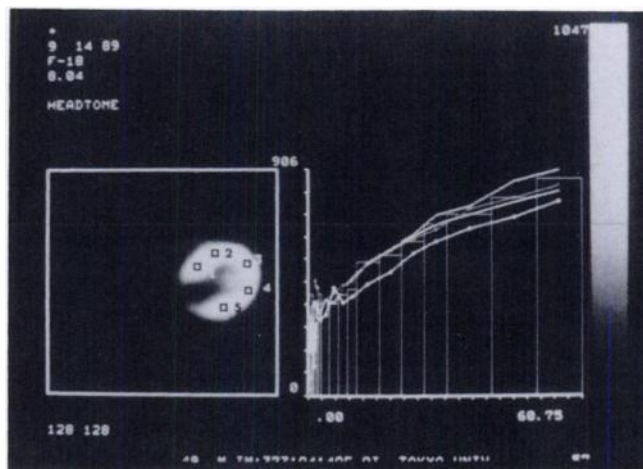


FIGURE 2. Left: Rectangular ROIs set on myocardium from septum, anterior wall to lateral wall. The patient is the same as in Figure 1. Right: Myocardial time-activity curves obtained from these ROIs (four lines and one bar graph). The early peak is the result of spillover of radioactivity from the left ventricular blood pool-to-myocardium.

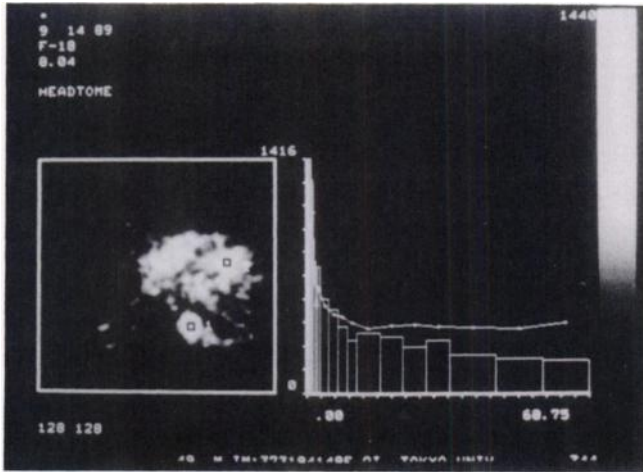


FIGURE 3. Left: Rectangular ROIs set on descending aorta and left ventricular blood pool of the same patient as in Figure 1. Left ventricular cavity is narrowed because of myocardial hypertrophy. Right: FDG time-activity curves obtained from these ROIs. At the later phase, the curve of the left ventricular blood pool is obviously elevated by spillover from myocardium. In this patient, the aortic cavity is large enough and the partial volume effect on the aortic curve is negligible.

descending aortic count as R_{hij} in Equation 2. Corrected venous count was substituted for arterial count by using Equation 1.

$$R_{hij} = A_i/D_{hi} = M_{ij} \cdot V_i/D_{hi}, \quad \text{Eq. 2}$$

where D_{hi} is the count of the smoothed descending aortic curve at time i on slice h (h is from 1 to 7). R_{hij} , which results from the partial volume effect, has to be constant during the seven time points from time 1 (13 min 15 sec) to time 7 (55 min 45 sec). When an inappropriate M_{ij} is used, $M_{ij} \cdot V_i$ does not equal A_i and R_{hij} does not become constant. However, when j is suitable, R_{hij} becomes constant from time 1 to 7 and $M_{ij} \cdot V_i$ is almost equal to A_i .

TABLE 1
Sets of Constants To Correct Venous Count-to-Arterial Count

Set	M1j	M2j	M3j	M4j	M5j	M6j	M7j
1	1	1	1	1	1	1	1
2	1.04	1.03	1.025	1.02	1.015	1.01	1.005
3	1.08	1.06	1.05	1.04	1.03	1.02	1.01
4	1.12	1.09	1.075	1.06	1.045	1.03	1.015
5	1.16	1.12	1.1	1.08	1.06	1.04	1.02
6	1.2	1.15	1.125	1.1	1.075	1.05	1.025

$M_{ij} = A_i/V_i$ at time i in j set; A_i = arterial whole blood count at time i ; V_i = venous whole blood count at time i . Time 1: 13 min 15 sec; time 2: 18 min 15 sec; time 3: 23 min 15 sec; time 4: 28 min 15 sec; time 5: 35 min 45 sec; time 6: 45 min 45 sec; and time 7 = 55 min 45 sec.

M_{ij} : A_i/V_i decreases from time 1 to time 7 but differs among patients. We made six sets of constants from M_{i1} to M_{i6} by analogy with the actual A_i/V_i of the patients.

To find a suitable j , we calculated aR_{ij} , aR_j , and S_j using Equations 3–5.

$$aR_{ij} = \sum_{h=1}^7 R_{hij}/7 \quad \text{Eq. 3}$$

$$aR_j = \sum_{i=1}^7 aR_{ij}/7 \quad \text{Eq. 4}$$

$$S_j = \sum_{i=1}^7 (aR_{ij} - aR_j)^2/7 \quad \text{Eq. 5}$$

When S_x was the smallest among S_1 – S_6 , i.e., aR_{ix} was the most constant from time 1 to time 7, M_{ix} turned out to be the most suitable set among M_{i1} – M_{i6} , and $M_{ix} \cdot V_i$ was almost equal to A_i . Thus, we could substitute V_i for A_i by determining a suitable M_{ij} without arterial sampling.

To correct for the partial volume effect, Ph was calculated using Equation 6.

$$Ph = \sum_{i=1}^7 R_{hix}/7 = \sum_{i=1}^7 M_{ix} \cdot V_i/(D_{hi} \cdot 7) \quad \text{Eq. 6}$$

The smoothed time-activity curve of the descending aorta on slice h was multiplied by Ph . The seven curves from seven slices corrected for partial volume effect were averaged to one curve [$I_w(t)$].

To correct the whole-blood value to the plasma value, R_b and $R_a(t)$ were calculated by Equations 7 and 8.

$$R_b = \sum_{i=1}^7 E_i/7A_i = \sum_{i=1}^7 F_i/7V_i \quad \text{Eq. 7}$$

where E_i is arterial plasma count at time i and F_i is venous plasma count at time i . Fortunately, E_i/A_i and F_i/V_i were almost the same and were constant from time 1 to time 7 (Table 2).

$$\begin{aligned} R_a(t) = 1: & \text{from } t = 0 \text{ to the peak time} \\ & = 1.02 - 1.13 : \text{from the peak time to 180 sec} \\ & \text{after the peak time (time B) (Table 2)} \\ & = 1: \text{later than time B} \end{aligned} \quad \text{Eq. 8}$$

$R_a(t)$ was defined to correct for the ratio between plasma and whole blood counts around the peak.

Input function [$I_p(t)$] was calculated by using Equation 9.

$$I_p(t) = R_a(t) \cdot R_b \cdot I_w(t) \quad \text{Eq. 9}$$

TABLE 2
Ratio Between Plasma and Whole Blood Counts (P/W ratio)

Average P/W ratio from 13 to 55 min (B ratio) (n = 10)	Venous blood	Arterial blood
	1.086 ± 0.031	1.090 ± 0.016
P/W ratio around the peak (A ratio) —the ratio of A ratio to B ratio (n = 10)		
at peak time		1.037 ± 0.045
15 sec after the peak		1.126 ± 0.103
30 sec after the peak		1.071 ± 0.065
45 sec after the peak		1.061 ± 0.042
60 sec after the peak		1.042 ± 0.026
90 sec after the peak		1.040 ± 0.016
120 sec after the peak		1.027 ± 0.010
180 sec after the peak		1.015 ± 0.014

Corrections

All data were corrected for the effects of the scanner's deadtime so as to reduce the error to less than 1%. In order to correct for the partial volume effect associated with object size, recovery coefficients (RC) obtained experimentally from phantom studies were used. RC was 0.8 in a 9-mm myocardial wall. RC was not used in the case of hypertensive diffuse hypertrophy, because the myocardial wall was thick enough.

Calculation of Regional Tissue Glucose Utilization

The three-compartment FDG tracer-kinetic model was used in the present study. The regional tissue glucose utilization rate (rTGU) can be calculated as $rTGU = (C_p/LC)k_1k_3/(k_2 + k_3)$. C_p is the plasma concentration of glucose; LC is the lumped constant that accounts for differences in the transport and phosphorylation of FDG and glucose (6, 9). In this study, LC was assumed to be a constant equal to 0.67 in myocardium (14). To estimate rTGU, Patlak graphic analysis was employed (7-8).

The dephosphorylation rate constant (k_4) of FDG has been assumed to be zero. $A_m(t)$ is tissue activity at time t , $C_p(t)$ is plasma activity at time t , and W is a function of the steady-state volume of the reversible compartments and effective plasma volume. A plot of $A_m(t)/C_p(t)$ versus $\int_0^t C_p(s)ds/C_p(t)$ should give a linear relationship at late times with a slope equal to $k_1k_3/(k_2 + k_3)$, and a y-intercept equal to W . Thus, this graphic approach enabled rTGU to be calculated by providing a direct estimate of $k_1k_3/(k_2 + k_3)$ from the slope of the linear relationship on the spot.

Tissue activities at seven separate time points (from 13 min 15 sec to 55 min 45 sec) were used to estimate the slope in Patlak analysis (Fig. 4). To compare estimates of the slope based on the arterial plasma input function to those based on the corrected aortic input function, Patlak analysis was repeated using the corrected aortic time-activity curve as the input function.

RESULTS

Ratio of the Plasma Count-to-the Whole-Blood Count

The ratios of the plasma count-to-the whole blood count (P/W ratio) from 13 min 15 sec to 55 min 45 sec were almost constant in both arterial blood and venous blood. The average P/W ratio of these seven time points was almost the same in venous and arterial blood (Table 2). The P/W ratio within 3 min after peak time (A ratio) was larger than the average P/W ratio from the 13 min to 55 min period (B ratio) (Table 2). From 4 min after the peak, the P/W ratio was almost the same as the B ratio. Figure 5 shows the plasma and whole blood curves of a patient as determined by arterial sampling.

Ratio Between Arterial and Venous Whole Blood Counts

The average ratio between arterial and venous whole blood counts (A/V ratio) is shown in Table 3. As mentioned previously, we defined six sets of constants from 1 to 6 (Table 1). The A/V ratio obtained from the seven aortic time-activity curves and venous whole blood counts are shown in Table 4. This A/V ratio was not so different from the one obtained by measurement.

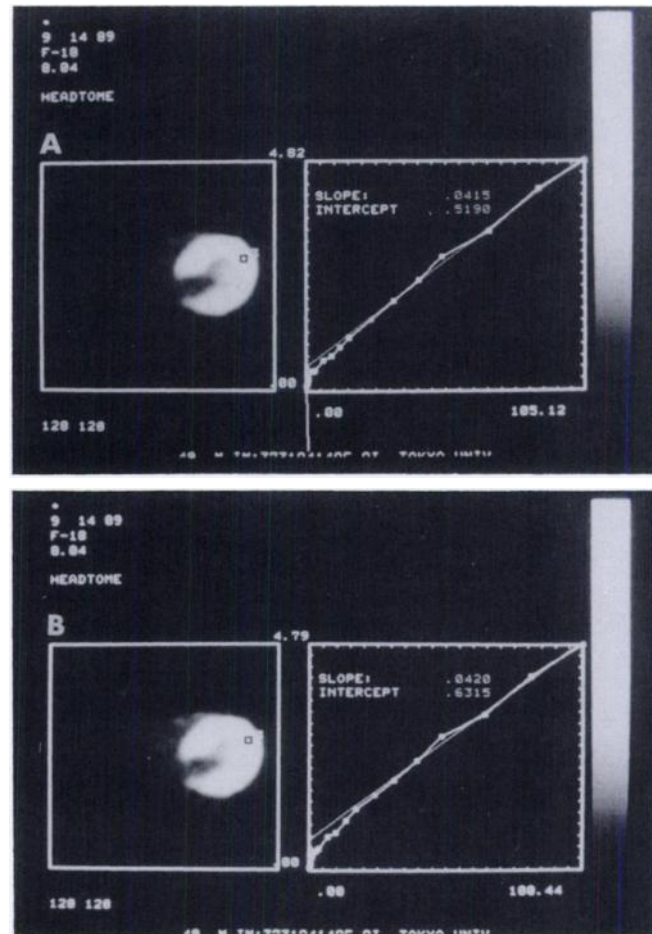


FIGURE 4. (A) Patlak analysis of myocardium of the same patient as in Figure 1 using the input function obtained from the corrected descending aortic curve. Slope represents $k_1k_3/(k_2 + k_3)$. (B) Patlak analysis of myocardium for the same ROI as in Figure 4A using the plasma input function obtained from arterial sampling. The value of $k_1k_3/(k_2 + k_3)$ is almost the same as that in Figure 4A.

Comparison Between Plasma and Aortic Time-Activity Curves

The constants (Ph) used to correct partial volume effect increased as the slices became lower, which is in keeping with the tendency for the descending aortic diameter to decrease as the slices become lower. The difference in counts between the calculated and measured plasma curves (Table 5) was about 10% around the peak but less than 3% beyond 18 min. The raw time-activity curve of the descending aorta, the curve corrected for partial volume effect, and the P/W ratio compared with the plasma and whole blood counts obtained by arterial sampling from one patient are shown in Figure 5.

Comparison of Patlak Analysis Using Two Different Input Functions

The $k_1k_3/(k_2 + k_3)$ values obtained by Patlak analysis using the plasma input function and the input function from the corrected aortic curve were in excellent agreement ($y = -0.00041 + 1.019x$, $r = 0.9995$, $n = 50$) (Fig.

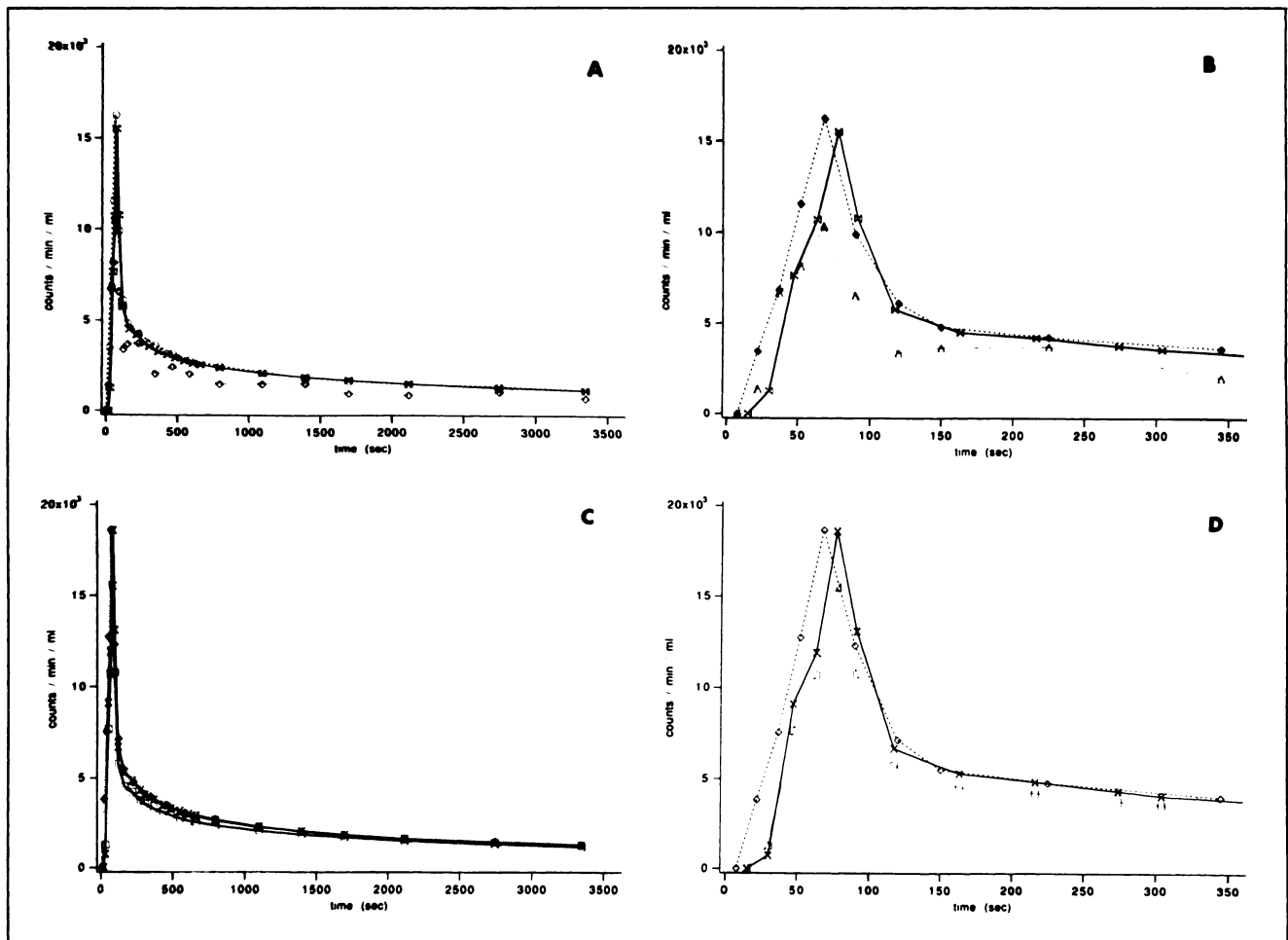


FIGURE 5. (A) A raw time-activity curve of descending aorta ($-\diamond-$), curve corrected for partial volume effect and averaged among seven curves ($-\circ-$), and curve of whole blood count of sampled arterial blood ($-\times-$). The raw curve is affected by noise and decreased by the partial volume effect. The curve averaged and corrected for the partial volume effect is almost the same as that for the whole blood count, especially in later phase, although they are slightly different around the peak. (B) The peak region of Figure 5A is expanded in this graph. The mark ($-\circ-$) is changed to the mark ($-\diamond-$) and the mark ($-\diamond-$) is changed to the mark ($-\Delta-$) in this graph. (C) A plasma time-activity curve for sampled arterial blood ($-\times-$), curve for the whole blood count of sampled arterial blood ($-\square-$) and the corrected curve for the descending aorta ($-\diamond-$). The whole blood count is lower than the plasma count throughout. The corrected curve is almost the same as the plasma curve. (D) The peak region of Fig. 5C is expanded in this graph.

6). The average difference between the two values was $2.32\% \pm 1.76\%$, and the difference for 48 of 50 values was less than 5%.

DISCUSSION

The purpose of this study was to demonstrate a noninvasive method for the quantification of rTGU by obtaining the input function without arterial sampling. Gambhir et al. used the left ventricular time-activity curve from dynamic PET data as the input function for that purpose (11). There were, however, several drawbacks to their method.

The first was spillover from other organs. In a Patlak analysis of an FDG study, it is of vital importance to obtain the correct input function in the later phase from 15 min to 60 min. Spillover from myocardium to left ventricle ascending aorta or atrium may cause an increase

in the count at that phase of the time-activity curve (Fig. 3). With our method, spillover from other organs to the descending aorta was negligible.

A second drawback to the Gambhir's method is the difference between the plasma and whole blood counts.

TABLE 3
Ratio Between Arterial and Venous Whole Blood Counts

Time after injection	Mean \pm s.d. (n = 10)
13 min 15 sec	1.089 \pm 0.060
18 min 15 sec	1.064 \pm 0.042
23 min 15 sec	1.054 \pm 0.043
28 min 15 sec	1.047 \pm 0.022
35 min 45 sec	1.041 \pm 0.041
45 min 45 sec	1.018 \pm 0.011
55 min 45 sec	1.006 \pm 0.006

TABLE 4
Measured Ratio Set versus Calculated Ratio Set Between Arterial and Venous Whole Blood Counts

Measured Calculated	1	2	3	4	5	6
1	3	0	0	0	0	0
2	0	0	1	1	0	0
3	0	0	1	1	0	0
4	0	0	0	1	1	0
5	0	0	0	0	0	0
6	0	0	0	0	1	0

Ratio sets from Mi1 to Mi6 are shown in Table 1. The calculated ratio set between arterial and venous whole blood counts was not much different from the measured ratio set.

Gambhir et al. reported that the whole blood count quickly became equal to the plasma count (11), a finding not confirmed by our results. In all ten patients whole blood count remained lower than plasma count throughout the study period. However, we were able to correct the curve to the plasma value.

The third point relates to partial volume effect. The partial volume effect does not cause much trouble in the left ventricle, ascending aorta and atrium, because their diameter is sufficient. However, in the descending aorta, the decrease in count caused by the partial volume effect cannot be ignored.

We calculated the partial volume effect by comparing the time-activity curve with venous sampling data obtained from 13 min to 55 min. Although arterial and venous blood counts sometimes differed, the difference could be estimated by our method.

Another problem is statistical error. Our three-point smoothing of each time-activity curve and averaging of

TABLE 5
Difference Between the Plasma Input Function Obtained by Arterial Sampling and That Calculated from the Aortic Time-Activity Curve

Time after injection	Difference
at peak time	9.29% ± 5.73%
2 min 30 sec	6.02% ± 3.29%
3 min 45 sec	5.57% ± 2.75%
5 min 45 sec	3.75% ± 2.65%
7 min 45 sec	5.29% ± 2.76%
9 min 45 sec	5.64% ± 4.13%
13 min 15 sec	4.72% ± 2.94%
18 min 15 sec	2.86% ± 2.49%
23 min 15 sec	2.57% ± 1.96%
28 min 15 sec	1.95% ± 1.82%
35 min 45 sec	2.19% ± 1.43%
45 min 45 sec	1.78% ± 1.72%
55 min 45 sec	2.87% ± 2.07%

Difference: mean ± s.d. of absolute difference if the difference for patient A is 9% and that for patient B is -10%, the mean will be 9.5%, not -0.5%.

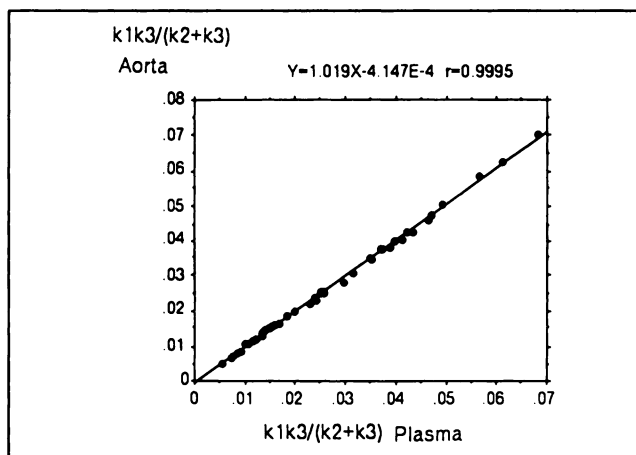


FIGURE 6. Plot of $k1k3/(k2 + k3)$ obtained by Patlak analysis using the input function obtained from the corrected aortic curve [$k1k3/(k2 + k3)$ Aorta] and the plasma input function determined from arterial sampling [$k1k3/(k2 + k3)$ Plasma]. There is good agreement ($r = 0.9995$) between estimates made by the two techniques. $y = -0.00041 + 1.019x$. $n = 50$ (five ROIs of ten patients).

seven time-activity curves obtained from the seven PET slices provided a solution. In ascending aorta and atrium, where the numbers of corresponding slices are very limited, the averaging is not effective.

We would emphasize that our method can be applied not only to myocardium but also to other thoracic and abdominal organs, because the descending aorta is present in the planes of these organs.

Furthermore, in the presence of valvular regurgitation or shunting, time-activity curves such as those of the left ventricle and atrium deviate from the arterial FDG concentration, a problem not encountered with our method.

There are some problems in Patlak analysis and in calculating rMGU as Gambhir et al. described (11), such as the correction for a positive $k4$. Although we did not estimate the error in rMGU caused by a positive $k4$, we believe it to be in line with Gambhir et al.'s report (11). Secondly, the partial-volume effect in the target tissue could be improved by using recovery coefficients based on regional assessments of myocardial wall thickness, which can be measured with echocardiography as Gambhir et al. described (11). Cardiac movement caused by beating and respiratory motion may influence the count of the target tissue, an effect that may be very difficult to correct. However, spillover from the cardiac chambers to the tissue is not a problem with Patlak analysis, since it affects only the y intercept and not the slope and thus does not influence estimates of rMGU.

Patient movement is a practical problem for all methods. To quantify glucose utilization accurately, a patient must remain motionless for the 1.50 hr needed for transmission and emission scanning. Patients often complain of hip, back, shoulder, or arm pain. We allowed patients to place sponges under hip, back, shoulder and arm.

Data processing time is another problem. It takes 10 to 15 min to acquire seven time-activity curves for the descending aorta. We used a personal computer (NEC PC9801) to correct these time-activity curves and obtain the input function, a process which took about 10 min. Patlak analysis of 6 or 7 ROIs of myocardium requires about 15 min.

In conclusion, this study demonstrated that the input function could be calculated noninvasively and accurately by time-activity curves of the descending aorta derived from dynamic PET data and venous sampling. Then, by using this input function, $k_1k_3/(k_2 + k_3)$ and regional glucose utilization could be estimated by the Patlak method. This method can be applied not only to heart but also to other thoracic and abdominal organs.

REFERENCES

1. Phelps ME, Hoffman EJ, Selin CE, et al. Investigation of (F-18)2-fluoro-2-deoxyglucose for the measurement of myocardial glucose metabolism. *J Nucl Med* 1978;19:1311-1319.
2. Marshall RC, Tillish JH, Phelps ME, et al. Identification and differentiation of resting myocardial ischemia and infarction in man with positron computed tomography, F-18-labeled fluorodeoxyglucose and N-13 ammonia. *Circulation* 1983;67:766-777.
3. Brunken R, Tillish J, Schwaiger M, et al. Regional perfusion, glucose metabolism and wall motion in chronic electrocardiographic Q-wave infarctions. Evidence for persistence of viable tissue in some infarct regions by positron emission tomography. *Circulation* 1986;73:951-963.
4. Brunken R, Schwaiger M, Grover-Mckay M, et al. Positron emission tomography detects tissue metabolic activity in myocardial segments with persistent thallium perfusion defects. *J Am Coll Cardiol* 1987;10:557-567.
5. Schwaiger M, Brunken R, Grover-Mckay M, et al. Regional myocardial metabolism in patients with acute myocardial infarction assessed by positron emission tomography. *J Am Coll Cardiol* 1986;8:800-808.
6. Sokoloff L, Reivich M, Kennedy C, et al. Tomographic measurement of local cerebral glucose utilization: theory, procedure, and normal values in the conscious and anesthetized albino rat. *J Neurochem* 1977;28:897-916.
7. Patlak CS, Blasberg RG, Fenstermacher JD. Graphical evaluation of blood-to-brain transfer constants from multiple-time uptake data. *J Cereb Blood Flow Metab* 1983;3:1-7.
8. Patlak CS, Blasberg RG. Graphical evaluation of blood-to-brain transfer constants from multiple-time uptake data. Generalizations. *J Cereb Blood Flow Metab* 1985;5:584-590.
9. Phelps ME, Huang SC, Hoffman EJ, et al. Tomographic measurement of local cerebral glucose metabolic rate in humans with (¹⁸F)2-fluoro-2-deoxy-d-glucose: validation of method. *Ann Neurol* 1979;6:371-388.
10. Huang SC, Phelps ME, Hoffman EJ, et al. Noninvasive determination of local cerebral metabolic rate of glucose in man. *Am J Physiol* 1980;238:E69-E82.
11. Gambhir SS, Schwaiger M, Huang SC, et al. Simple noninvasive quantification method for measuring myocardial glucose utilization in humans employing positron emission tomography and fluorine-18-deoxyglucose. *J Nucl Med* 1989;30:359-366.
12. Ehrenkauser RE, Potocki JF, Jewett DM, et al. Simple synthesis of F-18 labeled 2-fluoro-2-deoxy-D-glucose. *J Nucl Med* 1984;25:333-337.
13. Kanno I, Iida H, Miura S, et al. Design concepts and preliminary performances of stationary-sampling whole-body high-resolution positron emission tomograph: HEADTOME IV. *Jpn J Nucl Med* 1989;26:477-485.
14. Ratib O, Phelps ME, Huang SC, et al. Positron tomography with deoxyglucose for estimating local myocardial glucose metabolism. *J Nucl Med* 1982;23:577-586.